Assembly of Colloidal Nanoparticles Directed by the Microstructures of Polycrystalline Ice

Xiaoshuang Shen, Liyong Chen, Dehui Li, Liangfang Zhu, Hong Wang, Cuicui Liu, Yong Wang, Qihua Xiong, and Hongyu Chen*

Division of Chemistry and Biological Chemistry, Nanyang Technological University, Singapore 637371 and Division of Physics and Applied Physics, Nanyang Technological University, Singapore 637371

ABSTRACT We show that the microstructures of polycrystalline ice can serve as a confining template for one-dimensional assembly of colloidal nanoparticles. Upon simply freezing an aqueous colloid, the nanoparticles are excluded from ice grains and form chains in the ice veins. The nanoparticle chains are transferable and can be strengthened by polymer encapsulation. After coating with polyaniline shells, simple sedimentation is used to remove large aggregates, enriching single-line chains of 40 nm gold nanoparticles with a total length of several micrometers. When gold nanorods were used, they formed one-dimensional aggregates with specific end-to-end conformation, indicating the confining effects of the nanoscale ice veins at the final stage of freezing. The unbranched and ultralong plasmonic chains are of importance for future study of plasmonic coupling and development of plasmonic waveguides.

KEYWORDS: nanoparticle assembly · polycrystalline ice · template · one-dimensional · superstructure

Assembly of nanoparticles (NPs) into designed superstructures is of great importance for exploiting their collective properties.[1−4] It bridges the gap between individual NPs and the structures suitable for device applications.[5−8] In particular, one-dimensional (1D) superstructures of NPs have garnered much interest due to their anisotropic structure and unique properties.[9−15] For example, electromagnetic energy can propagate in the 1D arrays of metal NPs *via* the coupling of surface plasmons among adjacent NPs.[16,17] The propagation can be tailored and optimized by tuning the structural parameters, in particular the interparticle junctions. The nanoscale lateral dimension of the 1D NP arrays allows the propagation of electromagnetic energy below the diffraction limit of light, whereas the large longitudinal dimension makes them more manageable for use in optical or electric devices.[18,19]

Great efforts have been devoted to the fabrication of 1D NP assemblies. A popular approach is to introduce 1D templates,[20,21] such as DNA,[22] carbon nanotubes,[23] block copolymer micelles,[24] and other types of nanofibrils.[25−27] NPs usually randomly attach to the surface of these templates, making it difficult to achieve closely packed NP arrays. A different approach is to utilize the intrinsic interactions of NPs to achieve 1D aggregates. Magnetic[28−31] and electric[32,33] dipole interactions can linearly align NPs, and electrostatic repulsion favors the end-on attachment of a NP to a chain.[34−36] However, these intrinsic interactions cannot completely limit the freedom of NPs during their random aggregation,[37−40] and thus, branching is a constant problem, especially in forming long chains. Furthermore, there is no effective means to tune the width and cross section of the chains. Despite the recent progress, it remains a great challenge to fabricate long chains with minimal defects. In particular, achieving consistent contact junctions between the adjacent NPs in a chain is a greater challenge for exploiting their collective properties.

Here, we report a new assembly strategy using the microstructures of polycrystalline ice (PCI) as a confining template. Through simply freezing aqueous solution of NPs, 1D superstructures with a uniform cross section can be obtained. At the early stage of freezing, NPs, being impurities, are excluded from ice grains and concentrated in the liquid phase among them. As revealed by the works in the field of glaciology,[41−43] at a temperature near but below the freezing point, an interconnected system of water-filled veins can form in PCI. The veins lie along the lines where three ice grains meet, and thus, they take on a shape of a triangular prism (Figure 1). The unique characteristic of the veins is that their length can reach the macroscale, while their widths are dynamically adjustable and can reach the nanoscale at the final stage of freezing.

* Address correspondence to hongyuchen@ntu.edu.sg.

Received for review September 2, 2011 and accepted September 25, 2011.

Published online September 26, 2011
10.1021/nn203399z

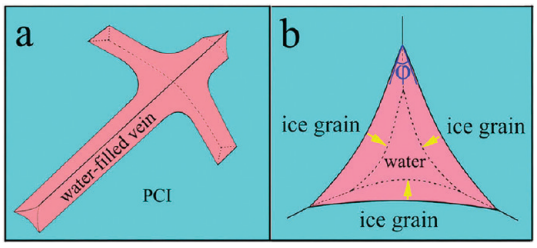

Figure 1. Schematic diagrams showing the microstructures of polycrystalline ice (PCI): (a) water-filled veins in PCI; four veins meet in a node at a four-grain intersection in PCI; and (b) cross section of a vein showing the triangular prism structure with their faces curved inward. Further freezing causes the vein to progressively shrink, as indicated by the arrows and dotted lines.

Thus, shrinking of the veins can confine the colloidal NPs therein to form superstructures dictated by the shape of the veins. The length of the products can reach two thousand NPs, while the width can be as thin as one NP.

RESULTS AND DISCUSSION

We demonstrate the method using aqueous solutions of spherical 40 nm gold NPs (AuNPs), which were synthesized by the citrate reduction method.[44,45] After centrifugation to remove the supernatant, the isolated AuNPs were redispersed in water to desired concentrations. Then, 20 μL of the solution was dropped onto a chip of silicon wafer, which was incubated at -20 °C for 30 min. The red solution turned to almost colorless ice (see the photographs in the Figure S1),[46] indicating the aggregation of the AuNPs. The aggregation was irreversible, as the solution remained colorless after the ice thawed. Finally, the sample was left to dry completely at room temperature and characterized by scanning electron microscopy (SEM).

Figure 2a provides a low-magnification SEM image of the products obtained with $\sim 6 \times 10^{10}$ particles/mL AuNP solution.[45] Most of them are 1D chains, accompanied by a few large 3D structures (Figure 2b,c; see discussion below). Some of the 1D structures found in this sample have a length of more than 100 μm, which is about 2500 times that of the NP diameter. The AuNPs always pack closely together in the chains. One of the long chains is shown in Figure 2d, with a magnified section in Figure 2e. It is entirely made of AuNPs, with a uniform width of about 5 NPs. Although its surface is rough, the overall shape of the triangular prism can be discerned. About 80% of the NP chains in this sample are found to have widths smaller than 5 NPs. Among them, the typical single-, double-, triple-, and quadruple-line chains of AuNPs are shown in Figure 2f–i, respectively. Even for the narrow single- and double-line chains, their length can reach tens of micrometers.[46] Branching rarely occurred in any of the chains except from a node. While the width of the chains was not constant, within an individual chain the width was remarkably uniform. In the single-line chains (Figure 2f), very few AuNPs bulged out and most of them formed linear alignment with their two neighbors. Another prominent characteristic of these chains was that they show a strong tendency to take a triangular prism shape, an evidence for the steric confinement of the nanoscale veins (*vide infra*). This was true even in the triple-line chains (Figure 2h), which is the smallest one that can exhibit such a shape. In chains of larger diameter (Figure 2e), slightly inward curved faces can be observed.

It was known that single-line AuNP chains with lengths of 100–300 nm absorb at around 700–800 nm.[36,47] Thus, the ultralong chains in our system should absorb far into the near-infrared (NIR). This explains the loss of color after freezing. The large superstructures appeared black as they formed precipitate in the thawed solution.

Obviously, the size of the AuNP chains should depend on the initial concentration of AuNPs. When the concentration was increased from 6×10^{10} to 3.8×10^{12} particles/mL, most of the resulting superstructures were found to have a larger diameter than those described above.[46] A small section of a typical chain is shown in Figure 3a. Its width was about 450 nm, and the triangular prism shape was clearly exhibited. We also observed AuNP superstructures forming a complete node with four veins still attached (Figure 3b). It was very similar in structure to the nodes observed in PCI (Figure 1a).[42] When the initial concentration of AuNPs was decreased to $\sim 3.8 \times 10^9$ particles/mL, only short chains with narrow width were obtained.[46] The AuNPs were probably not of sufficient quantity to fill the entire vein at the final stage of freezing. The resulting short chains of AuNPs separated when the ice melted.

The veins in PCI are known to have a triangular prism shape with concave faces (Figure 1). Their width is usually uniform though with varying sizes.[41–43] On the basis of the strong correlation between the structures of the observed products and those of the veins, we believe that the various superstructures of AuNPs were generated inside and templated by the veins in PCI. The smooth surface of the large structures (*e.g.*, Figure 3b) and the consistent surface curvature along the length of individual chains (Figure 3a) are clear signs of templating ice microstructures. Such spatial order cannot have been created by random aggregation of colloidal AuNPs.

Apparently, at the final stage of freezing, the width of the veins was comparable to that of the chains, so that the aggregating AuNPs were forced to conform to the shape of the veins. This confining capability of the veins is of great significance. There are two possible ways to form the single-line chains shown in Figure 2f: (1) the AuNPs might linearly aggregate inside the veins to form small clusters,[36,38] which were then squeezed together to form the long chain; or (2) the NPs might remain separated until they were squeezed together by the shrinking veins. The 1D clusters obtained by

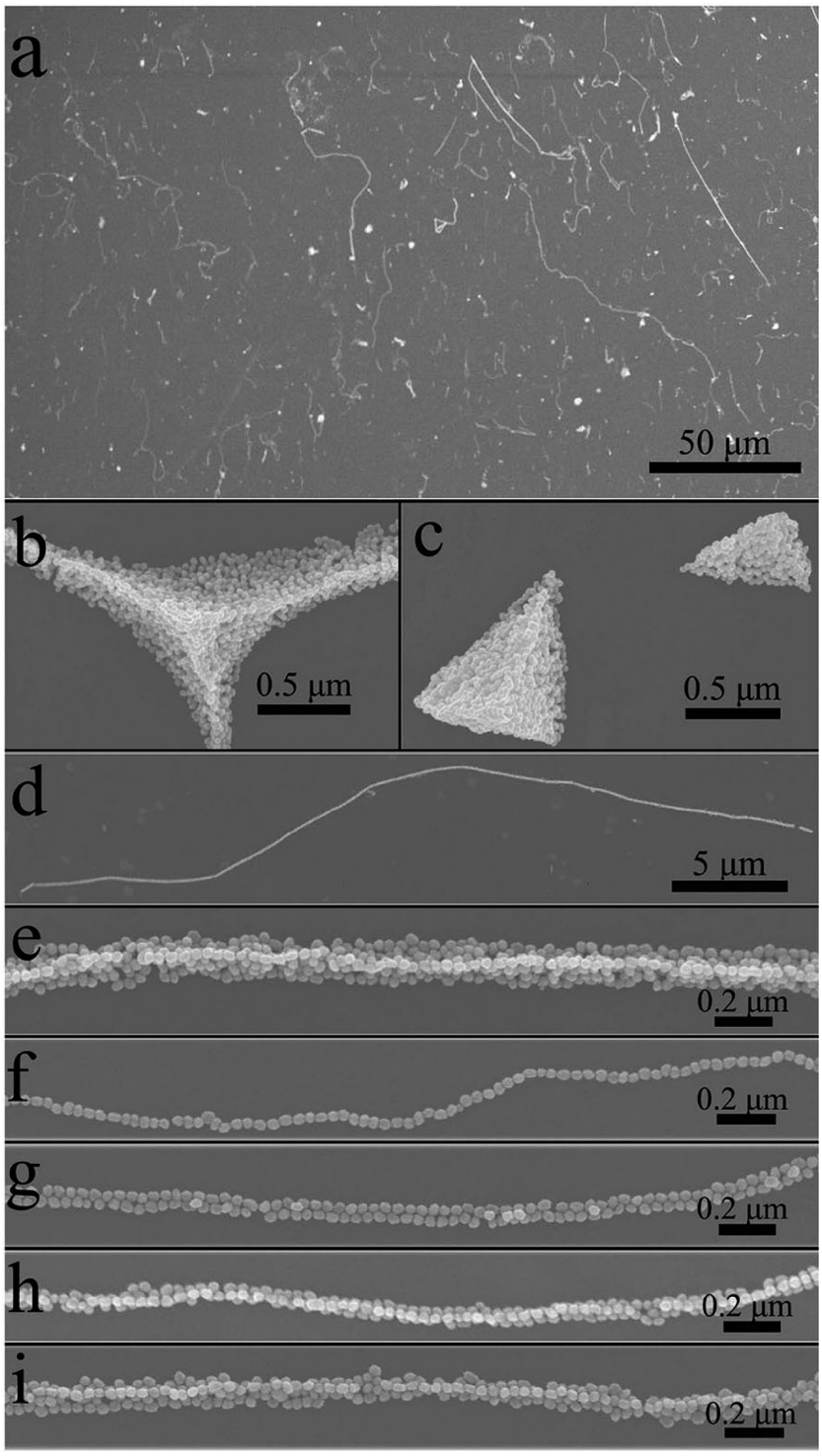

Figure 2. SEM images of the products obtained with ~6 × 10^{10} particles/mL of AuNP solution: (a) low-magnification SEM image of the products; (b, c) tetrahedral NP superstructures with concave and flat faces (see an additional image at a tilted angle in Figure S8[46]), respectively; (d) a long NP chain; (e) an enlarged section of d; (f–i) typical single-, double-, triple-, and quadruple-line chains, respectively. Triangular prism shape can be observed in e, h, and i.

aggregating citrate-stabilized AuNPs often have a high branching ratio,[36] and thus, our observation of smooth single-line chains favors the second mechanism.

To further study this issue, we used anisotropic Au nanorods (AuNRs) as building blocks. The as-synthesized AuNRs[48] were purified by centrifugation to remove the excess hexadecyltrimethylammonium bromide (CTAB); they were redispersed in water and then used for our freezing experiments. Among the products, single-line chains of AuNRs were observed (Figure 3c). Most of the AuNRs adopted end-to-end conformation with their neighbors, with only few AuNRs positioned perpendicular

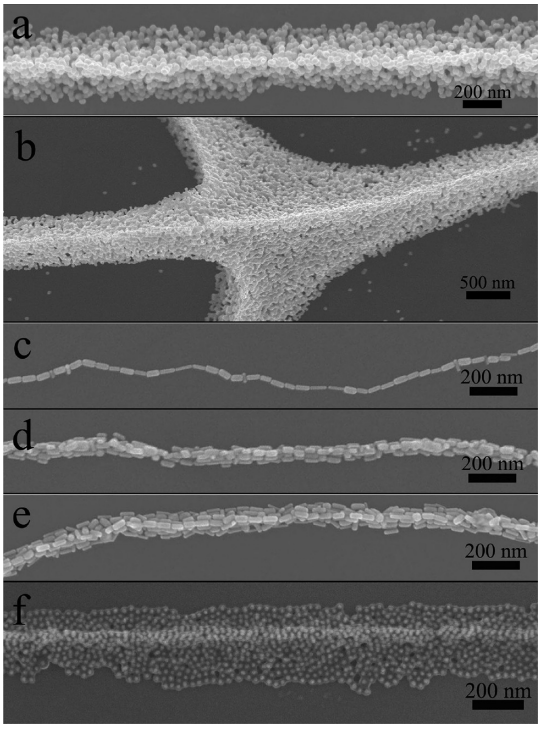

Figure 3. SEM images of the products obtained under different experimental conditions: (a, b) a typical chain and a node-shaped superstructure obtained with ~3.8 × 10^{12} particles/mL AuNP solution; (c−e) typical AuNR chains obtained with AuNR solution; (f) typical superstructure obtained with core−shell Au@PSPAA NP solution.

to the chain. Side-by-side conformation was extremely rare, and the angles between neighboring AuNRs were usually linear. To account for the highly ordered end-to-end aggregation, the AuNRs were most likely not aggregated until the vein size was comparable to the length of the AuNRs. We did not find any case where the AuNRs were arranged in a zigzag conformation. If the approaching ice walls could crush the zigzag chains, we should have been able to observe a large number of partially stacked conformations. Thus, the AuNRs should be able to move in the tiny veins with the liquid phase during the final stage of freezing. In the multiple-line chains of AuNRs, a triangular prism shape can also be identified (Figure 3d, e). One interesting feature is that most of the NRs have the same orientation; their long axes aligned along the longitudinal direction of the chains. This happened even when the width of the chain was larger than the length of the AuNRs. In this case, it was unlikely that the steric effect of the vein alone determined the AuNR's orientation. The steric influence from the neighboring AuNRs and/or the movement of the liquid phase may also contribute to their alignment. Our ability of controlling the orientation of AuNRs could be useful for tuning the collective properties of their superstructures.[49]

It should be noted that removal of excess salts (*e.g.*, sodium citrate) or surfactants (*e.g.*, CTAB) from the as-synthesized NP solutions is of importance. Like NPs, these chemicals are excluded from ice grains and concentrated in the veins. At high concentration, they could interfere with ice formation and/or cause the agglomeration of NPs before ice veins could exert steric influence.

The successful assembly of both citrate-stabilized AuNPs and CTAB-stabilized AuNRs demonstrated the generality of our assembly method. The method can also be applied to fabricate 1D superstructures with composite building blocks, such as the core@shell Au@PSPAA NPs (PSPAA = polystryrene-*block*-poly(acrylic acid), d_{Au} = 15 nm, $d_{overall}$ = 30 nm).[50] The interactions among these NPs are mainly determined by the polymer shells, especially by the negatively charged PAA chains.[51] As shown in the initial results (Figure 3f), triangular prism shaped superstructures also can be obtained, and the length can reach tens of micrometers.[46] An advantage of using core−shell NPs as building blocks is that the shell can be used as a uniform and tunable spacer. The gap distance between AuNPs is known to be of critical importance in determining the collective properties of their superstructures. Equally important, the fact that the NPs were embedded in and shielded by the polymer shell suggests that any types of NPs encapsulated by PSPAA[8,50,52−54] can be assembled using this method.

The formation of the vein system in PCI is homologous to the formation of Plateau borders in foams.[55] In both cases, minimization of the overall interfacial energy plays a key role. The equilibrium geometry of the vein is determined by the interfacial energy of the solid−liquid surface γ_{sl} and the grain-boundary energy γ_{ss} as follows:[42]

$$2\cos(\phi/2) = \gamma_{ss}/\gamma_{sl}$$

where ϕ is the dihedral angle of neighboring ice grains measured from inside the water-filled vein (marked in Figure 1b). In the foam system, the mobile liquid walls quickly equilibrated to make ϕ always equal to 60°,[55] whereas in PCI the local differences also played an important role in the kinetics of forming the solid ice grains. As analyzed by Nye and Frank,[56] for the dihedral angle $\phi < 60°$, the liquid phase in PCI forms a system of veins and nodes, while for $\phi > 60°$, the liquid phase resides in isolated pockets (not nodes) at four-grain intersections. More specifically, for $60° < \phi < 70°32'$, concave-faced tetrahedra are the most stable form of such intersections, while for $\phi = 70°32'$, flat-faced tetrahedra are the most stable. In PCI, the dihedral angle ϕ was found to range from 25° to 105° in a same sample.[42] The diversity was attributed to the local differences in the grain-boundary energy with the formation of ice crystals.

As mentioned above, large 3D superstructures of AuNPs were also observed in our products (Figure 2b,c) despite their rare occurrence. They took on tetrahedral shapes with either concave (Figure 2b) or flat (Figure 2c) faces. The close packing of their constituent AuNPs is indicative of compressive forces exerted by the approaching

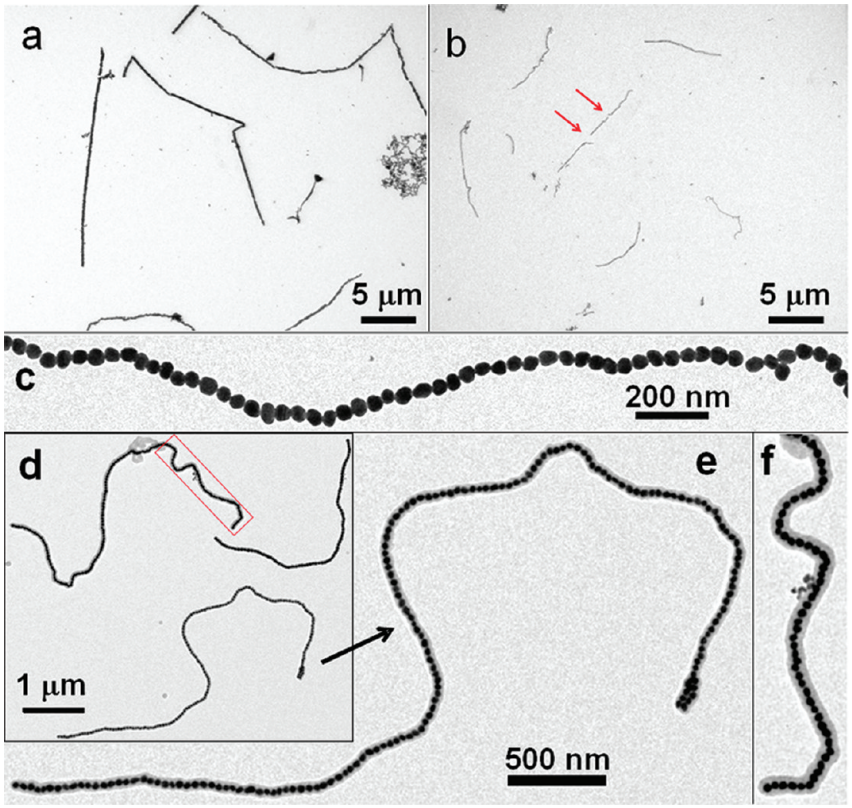

Figure 4. TEM images of the products obtained through freezing 500 μL of AuNP solution (a) in a −80 °C fridge and (b) in −80 °C ethanol; (c) a single-line chain observed in sample b; (d) single-line chains of sample b after being encapsulated by PANI and enriched by differential sedimentation; (e, f) the magnified sections in d.

ice walls during the freezing. These shapes were consistent with the predicted shapes of intersections as discussed above. Obviously, the local environment was different during the formation of structures in Figure 2b and c. Since the majority of the products obtained in our system were 1D superstructures and nodes, we concluded that the liquid phase in PCI mainly existed in veins instead of isolated pockets. This conclusion agrees with the previous observations in PCI.[41−43]

The above assembly method worked well when we froze 20 μL of solution directly on the surface of silicon chips. However, we encountered problems when we tried to scale up the synthesis: 500 μL of the solution (~6×10^{10} particles/mL) in a glass vial was frozen in a −20 °C fridge; the sample was thawed and a small aliquot (20 μL) transferred to a TEM (transmission electron microscopy) sample grid and then dried. The resulting sample showed thick AuNP chains (>100 nm in diameter) among other large microstructures.[46] Lowering the AuNP concentration did not significantly improve the assembly result. It should be noted that it took about 3 min to freeze the 20 μL of solution on a silicon chip, but 25 min for the 500 μL of solution in a glass vial. Hence, it appeared that the larger amount of solution and the thick glass wall might have slowed the rate of freezing and affected the NP assembly.

The slower rate of freezing can lead to larger ice grains. Probably, as ice grains grew, the solutions inside the veins became spatially isolated. The concentrations of the AuNPs trapped in the veins were thus not only dependent on the initial concentration of AuNPs. With water being depleted by freezing, the accumulated AuNPs in the veins were ultimately dependent on the size of the neighboring ice grains: Larger grain means greater volume of the initial solution. Thus, the remaining AuNPs were more concentrated in the veins next to larger ice grains. This explains our observation of large structures by slow freezing.

Two control experiments were conducted to increase the rate of freezing. In one experiment, 500 μL of the solution was frozen in a glass vial in a −80 °C fridge; in the other, the vial containing the same amount of solution was directly immersed in −80 °C ethanol (mp −117.3 °C) to accelerate the rate of heat exchange. It took about 10 and 2 min, respectively, to thoroughly freeze the solutions. The samples were thawed, transferred to TEM grids, dried, and then characterized. While AuNP chains were obtained in both cases, those obtained from the faster freezing were significantly smaller in diameter (Figure 4b vs 4a). Hence, the results were consistent with our expectations: The faster freezing gave rise to smaller ice grains in greater number; the resulting larger number of veins in PCI led to the formation of smaller AuNP chains.

In Figure 4a, a number of sharp-angle kinks could be observed. It appeared that the transfer of the thawed

sample may have introduced sheer forces and bent the long AuNP chains. This was in contrast to the relatively straight chains in Figure 2a, where the 20 μL sample was directly thawed and dried without much disturbance. In Figure 4b, however, sharp kinks were rare, but the chains were significantly shorter than those in Figure 4a. The small-width chains were more flexible but less robust. They probably have been broken in the solution. In a few cases, we observed gaps in the chains (indicated by arrows), with the separated parts still perfectly aligned. These gaps cannot have been formed in solution; they were most likely formed at the final stage of drying after the chains were adsorbed on the grid surface.

The fact that we obtained micrometer-length chains suggested that most of AuNP−AuNP junctions survived the sheer forces. To separate a 20 μm chain (about 500 AuNPs) into 2 μm pieces, only 2% of the junctions have to be broken. While single-line chains are fragile, we still observed a few chains several micrometers in length (Figure 4c). Obviously, the bonding between the aggregated AuNPs was relatively strong. Such strong bonding is not unique to this system: It is known that salt-induced aggregation of citrate-stabilized AuNPs is not reversible.[2,36] Longer chains are more exposed to shear forces and thus more breakable. While breaking by shear forces is a problem, it only occurs when the chains are long enough.

In order to preserve the long chains of AuNPs, particularly the single-line chains, we tried to strengthen the nanostructures by coating them with shells of conductive polymer, namely, polyaniline (PANI).[47] Briefly, aniline, sodium dodecylsulfate (SDS), and an acidic solution of $(NH_4)_2S_2O_8$ were mixed in a 1.5 mL tube, before the addition of 400 μL of thawed sample solution (the sample shown in Figure 4b).[46] The mixture was incubated for 24 h, during which the polymer shell formed and the large chains precipitated. Hence, the PANI-encapsulated small chains were enriched in the solution by differential sedimentation.[40] These remaining chains were collected by centrifugation, transferred *via* a pipet to a TEM grid, and then dried. As shown in Figure 4d−f (see more examples in the Supporting Information), the single-line chains were enriched in this sample, and their uniform polymer shells can be easily identified. Considering the long and harsh treatments, it was remarkable that single-line AuNP chains over 5 μm in length could be preserved. After the ice-induced assembly, the sample was thawed, transferred, treated with acid and surfactant (SDS) during the 24 h polymerization, centrifuged, transferred again, and then dried. In this sample, although the chains were highly curved, sharp kinks and open gaps were rare, highlighting the protective role of the polymer shells. The shells also preserved the AuNP aggregates as they were in the solution, confirming that the chains were not formed by the drying process of SEM/TEM sample preparation. After purification, most of the large structures were removed, and thus the synthesis is not efficient in terms of yield. But to the best of our knowledge, this method produced single-line chains of AuNPs in record length.

Previously, 3D porous microstructures were obtained by directionally freezing solutions of NPs and graphene.[57−60] In these methods, concentrated NP solutions were used so that the shape of the frozen liquid or its droplets[60] was maintained by the solid substances being excluded from ice grains. Microwires of NPs resulted from this process were typically several hundred nanometers in diameter and formed an interconnected network. The directional freezing can establish control of microstructures in aligning the microwires. However, individual microwires were not obtained.

In contrast, our method used much lower concentrations of NPs so that the presence of NPs did not significantly disrupt the vein formation in PCI. Hence, most of the NPs were only concentrated in isolated veins at the final stage of freezing, resulting in the formation of individual 1D superstructures as thin as one AuNP in width. As demonstrated by the end-to-end alignment of AuNRs, the veins in PCI are a unique handle for precision engineering at the nanoscale. Thus, our approach provides novel capabilities in nanoparticle-level assembly, which is significantly smaller than the microwire network fabricated by the previous freezing method.

In the field of NP assembly, a prominent problem is the lack of means to control the random Brownian motion of NPs. Templates and intrinsic NP interactions have limited capability, often leading to loose assembly and branching. In contrast, the veins in PCI were formed progressively, reaching the nanoscale only at the final stage of freezing. Thus, the spatially confined AuNPs were forced together and packed closely into a 1D assembly. Importantly, the vein templates originated from the solution itself, eliminating the need to introduce foreign materials such as templates, ligands, and surfactants. These additives often have considerable effects on the properties of the resulting superstructures. The vein templates can be easily removed by melting the ice, leaving the AuNP superstructures suspended in the solution and available for further treatments. While the breaking of long chains is a problem, it should be noted that even the shortened single-line AuNP chains were longer than those reported in the literature. From this perspective, those obtained should be the longest chains that can survive in colloidal solutions. Polymer encapsulation is a convenient approach to extend the average length of such chains. The lack of branching is another feature of importance for device fabrication.

CONCLUSIONS

In summary, we report a new synthetic strategy for unbranched ultralong chains of nanoparticles, by exploiting the microstructures of polycrystalline ice as a confining template. To the best of our knowledge, such

nanoparticle chains are so far inaccessible by the existing means in the literature. The method is facile and general, and the resulting chains can be strengthened by polymer encapsulation. Our understanding of the involved mechanism is an important step toward exploring the potentials of this new method.

MATERIALS AND METHODS

Chemicals. All chemical reagents were used without further purification. Hydrogen tetrachloroaurate(III) hydrate, 99.9% (metal basis Au 49%), was purchased from Alfa Aesar; amphiphilic diblock copolymer polystyrene-*block*-poly(acrylic acid) (PS_{154}-*b*-PAA_{49}, M_n = 16 000 for the polystyrene block and M_n = 3500 for the poly(acrylic acid) block, M_w/M_n = 1.15) was purchased from Polymer Source, Inc.; all other chemicals were purchased from Aldrich.

Characterization. SEM images were collected from a JEOL-6700 scanning electron microscope operated at 10 kV. TEM images were collected from a JEM-1400 transmission electron microscope (JEOL) operated at 120 kV.

Assembly of AuNPs, AuNRs, and Core–Shell Au@PSPAA NPs. The assembly was achieved through simply freezing the aqueous solution of the corresponding NPs. Before being used, the 40 nm AuNPs were purified by centrifugation (2000*g*, 20 min) to remove the excess sodium citrate, before they were redispersed in DI water. The AuNRs and core–shell Au@PSPAA NPs were purified twice by centrifugation (8000*g*, 20 min). To freeze the solution, 20 μL of the corresponding solution was dropped onto a 4 mm × 4 mm chip of silicon wafer, which was then put in a −20 °C freezer for 30 min. After that, the sample was left at room temperature to melt the ice and completely vaporize the water.

For the preparation of the samples shown in Figure 4a and b, 0.5 mL of the AuNP solution was added in a 4 mL vial, which was then put in a −80 °C freezer or in a −80 °C ethanol solution for 30 min. After that, the samples were left at room temperature to melt the ice. Aliquots of 20 μL were transferred to TEM grids and dried.

Encapsulation of the 1D Chains with Polyaniline and Separation of the Polymer-Coated Chains. We use the encapsulation method developed by our group.[47] Briefly, a mixture of aniline (2 mM, 400 μL), sodium dodecylsulfate (40 mM, 40 μL), and $(NH_4)_2S_2O_8$ (2 mM in 10 mM HCl, 400 μL) was prepared first. Then, a 0.4 mL solution of 1D chains was added to the mixture. The reaction mixture was incubated at room temperature for 24 h without stirring for the polymerization reaction to complete. After this step, the heavier aggregates precipitated from the solution; the supernatant was transferred to a 1.5 mL tube and centrifuged (150*g*, 20 min), in order to isolate the remaining chains in the colloidal solution. The deposit was redispersed in 10 μL of water and then transferred to a TEM grid.

Acknowledgment. The authors thank the Division of Physics and Applied Physics, NTU, for SEM usage; and the MOE (ARC 13/09) and NRF (CRP-4-2008-06) of Singapore for financial support.

Supporting Information Available: Syntheses of AuNPs, AuNRs, and core–shell Au@PSPAA NPs; photographs of the samples before and after freezing; TEM and SEM images of the products obtained under different experimental conditions. This material is available free of charge *via* the Internet at http://pubs.acs.org.

REFERENCES AND NOTES

1. Nie, Z. H.; Petukhova, A.; Kumacheva, E. Properties and Emerging Applications of Self-Assembled Structures Made from Inorganic Nanoparticles. *Nat. Nanotechnol.* **2010**, *5*, 15–25.
2. Wang, Y.; Chen, G.; Yang, M. X.; Silber, G.; Xing, S. X.; Tan, L. H.; Wang, F.; Feng, Y. H.; Liu, X. G.; Li, S. Z.; *et al.* A Systems Approach towards the Stoichiometry-Controlled Hetero-Assembly of Nanoparticles. *Nat. Commun.* **2010**, *1*, 87.
3. Zhang, Z.; Wong, L. M.; Ong, H. G.; Wang, X. J.; Wang, J. L.; Wang, S. J.; Chen, H. Y.; Wu, T. Self-Assembled Shape- and Orientation-Controlled Synthesis of Nanoscale Cu_3Si Triangles, Squares, and Wires. *Nano Lett.* **2008**, *8*, 3205–3210.
4. Dong, H. C.; Zhu, M. Z.; Yoon, J. A.; Gao, H. F.; Jin, R. C.; Matyjaszewski, K. One-Pot Synthesis of Robust Core/Shell Gold Nanoparticles. *J. Am. Chem. Soc.* **2008**, *130*, 12852–12853.
5. Lee, J.; Hernandez, P.; Lee, J.; Govorov, A. O.; Kotov, N. A. Exciton-Plasmon Interactions in Molecular Spring Assemblies of Nanowires and Wavelength-Based Protein Detection. *Nat. Mater.* **2007**, *6*, 291–295.
6. He, L.; Hu, Y. X.; Kim, H.; Ge, J. P.; Kwon, S.; Yin, Y. D. Magnetic Assembly of Nonmagnetic Particles into Photonic Crystal Structures. *Nano Lett.* **2010**, *10*, 4708–4714.
7. Rosi, N. L.; Mirkin, C. A. Nanostructures in Biodiagnostics. *Chem. Rev.* **2005**, *105*, 1547–1562.
8. Dai, Q.; Berman, D.; Virwani, K.; Frommer, J.; Jubert, P. O.; Lam, M.; Topuria, T.; Imaino, W.; Nelson, A. Self-Assembled Ferrimagnet Polymer-Composites for Magnetic Recording Media. *Nano Lett.* **2010**, *10*, 3216–3221.
9. Tang, Z. Y.; Kotov, N. A. One-Dimensional Assemblies of Nanoparticles: Preparation, Properties, and Promise. *Adv. Mater.* **2005**, *17*, 951–962.
10. Muller, A. H. E.; Yuan, J. Y. One-Dimensional Organic-Inorganic Hybrid Nanomaterials. *Polymer* **2010**, *51*, 4015–4036.
11. Wang, F.; Han, Y.; Lim, C. S.; Lu, Y. H.; Wang, J.; Xu, J.; Chen, H. Y.; Zhang, C.; Hong, M. H.; Liu, X. G. Simultaneous Phase and Size Control of Upconversion Nanocrystals through Lanthanide Doping. *Nature* **2010**, *463*, 1061–1065.
12. Kang, Y. J.; Erickson, K. J.; Taton, T. A. Plasmonic Nanoparticle Chains *via* a Morphological, Sphere-to-String Transition. *J. Am. Chem. Soc.* **2005**, *127*, 13800–13801.
13. DeVries, G. A.; Brunnbauer, M.; Hu, Y.; Jackson, A. M.; Long, B.; Neltner, B. T.; Uzun, O.; Wunsch, B. H.; Stellacci, F. Divalent Metal Nanoparticles. *Science* **2007**, *315*, 358–361.
14. Jackson, A. M.; Myerson, J. W.; Stellacci, F. Spontaneous Assembly of Subnanometre-Ordered Domains in the Ligand Shell of Monolayer-Protected Nanoparticles. *Nat. Mater.* **2004**, *3*, 330–336.
15. Verma, A.; Uzun, O.; Hu, Y. H.; Hu, Y.; Han, H. S.; Watson, N.; Chen, S. L.; Irvine, D. J.; Stellacci, F. Surface-Structure-Regulated Cell-Membrane Penetration by Monolayer-Protected Nanoparticles. *Nat. Mater.* **2008**, *7*, 588–595.
16. Maier, S. A.; Kik, P. G.; Atwater, H. A.; Meltzer, S.; Harel, E.; Koel, B. E.; Requicha, A. A. G. Local Detection of Electromagnetic Energy Transport below the Diffraction Limit in Metal Nanoparticle Plasmon Waveguides. *Nat. Mater.* **2003**, *2*, 229–232.
17. Li, Z. P.; Bao, K.; Fang, Y. R.; Huang, Y. Z.; Nordlander, P.; Xu, H. X. Correlation between Incident and Emission Polarization in Nanowire Surface Plasmon Waveguides. *Nano Lett.* **2010**, *10*, 1831–1835.
18. Lee, D.; Choe, Y. J.; Choi, Y. S.; Bhak, G.; Lee, J.; Paik, S. R. Photoconductivity of Pea-Pod-Type Chains of Gold Nanoparticles Encapsulated within Dielectric Amyloid Protein Nanofibrils of alpha-Synuclein. *Angew. Chem., Int. Ed.* **2011**, *50*, 1332–1337.
19. Favier, F.; Walter, E. C.; Zach, M. P.; Benter, T.; Penner, R. M. Hydrogen Sensors and Switches from Electrodeposited Palladium Mesowire Arrays. *Science* **2001**, *293*, 2227–2231.
20. Grzelczak, M.; Vermant, J.; Furst, E. M.; Liz-Marzan, L. M. Directed Self-Assembly of Nanoparticles. *ACS Nano* **2010**, *4*, 3591–3605.
21. He, D.; Hu, B.; Yao, Q. F.; Wang, K.; Yu, S. H. Large-Scale Synthesis of Flexible Free-Standing SERS Substrates with High Sensitivity: Electrospun PVA Nanofibers Embedded with Controlled Alignment of Silver Nanoparticles. *ACS Nano* **2009**, *3*, 3993–4002.

22. Warner, M. G.; Hutchison, J. E. Linear Assemblies of Nanoparticles Electrostatically Organized on DNA Scaffolds. *Nat. Mater.* **2003**, *2*, 272–277.
23. Correa-Duarte, M. A.; Perez-Juste, J.; Sanchez-Iglesias, A.; Giersig, M.; Liz-Marzan, L. M. Aligning an Nanorods by Using Carbon Nanotubes as Templates. *Angew. Chem., Int. Ed.* **2005**, *44*, 4375–4378.
24. Wang, H.; Lin, W. J.; Fritz, K. P.; Scholes, G. D.; Winnik, M. A.; Manners, I. Cylindrical Block Co-Micelles with Spatially Selective Functionalization by Nanoparticles. *J. Am. Chem. Soc.* **2007**, *129*, 12924–12925.
25. Sharma, N.; Top, A.; Kiick, K. L.; Pochan, D. J. One-Dimensional Gold Nanoparticle Arrays by Electrostatically Directed Organization Using Polypeptide Self-Assembly. *Angew. Chem., Int. Ed.* **2009**, *48*, 7078–7082.
26. Chen, C. L.; Zhang, P. J.; Rosi, N. L. A New Peptide-Based Method for the Design and Synthesis of Nanoparticle Superstructures: Construction of Highly Ordered Gold Nanoparticle Double Helices. *J. Am. Chem. Soc.* **2008**, *130*, 13555–13557.
27. Chen, T.; Xing, G. Z.; Zhang, Z.; Chen, H. Y.; Wu, T. Tailoring the Photoluminescence of ZnO Nanowires Using Au Nanoparticles. *Nanotechnology* **2008**, *19*, 435711.
28. Butter, K.; Bomans, P. H. H.; Frederik, P. M.; Vroege, G. J.; Philipse, A. P. Direct Observation of Dipolar Chains in Iron Ferrofluids by Cryogenic Electron Microscopy. *Nat. Mater.* **2003**, *2*, 88–91.
29. Hu, Y. X.; He, L.; Yin, Y. D. Magnetically Responsive Photonic Nanochains. *Angew. Chem., Int. Ed.* **2011**, *50*, 3747–3750.
30. Hu, M. J.; Lu, Y.; Zhang, S.; Guo, S. R.; Lin, B.; Zhang, M.; Yu, S. H. High Yield Synthesis of Bracelet-Like Hydrophilic Ni-Co Magnetic Alloy Flux-Closure Nanorings. *J. Am. Chem. Soc.* **2008**, *130*, 11606–11607.
31. Lu, Y.; Zhao, Y.; Yu, L.; Dong, L.; Shi, C.; Hu, M. J.; Xu, Y. J.; Wen, L. P.; Yu, S. H. Hydrophilic Co@Au Yolk/Shell Nanospheres: Synthesis, Assembly, and Application to Gene Delivery. *Adv. Mater.* **2010**, *22*, 1407–1411.
32. Tang, Z. Y.; Kotov, N. A.; Giersig, M. Spontaneous Organization of Single CdTe Nanoparticles into Luminescent Nanowires. *Science* **2002**, *297*, 237–240.
33. Tang, Z. Y.; Ozturk, B.; Wang, Y.; Kotov, N. A. Simple Preparation Strategy and One-Dimensional Energy Transfer in CdTe Nanoparticle Chains. *J. Phys. Chem. B* **2004**, *108*, 6927–6931.
34. Zhang, H.; Wang, D. Y. Controlling the Growth of Charged-Nanoparticle Chains through Interparticle Electrostatic Repulsion. *Angew. Chem., Int. Ed.* **2008**, *47*, 3984–3987.
35. Zhang, H.; Fung, K. H.; Hartmann, J.; Chan, C. T.; Wang, D. Y. Controlled Chainlike Agglomeration of Charged Gold Nanoparticles *via* a Deliberate Interaction Balance. *J. Phys. Chem. C* **2008**, *112*, 16830–16839.
36. Yang, M. X.; Chen, G.; Zhao, Y. F.; Silber, G.; Wang, Y.; Xing, S. X.; Han, Y.; Chen, H. Y. Mechanistic Investigation into the Spontaneous Linear Assembly of Gold Nanospheres. *Phys. Chem. Chem. Phys.* **2010**, *12*, 11850–11860.
37. Chen, T.; Wang, H.; Chen, G.; Wang, Y.; Feng, Y. H.; Teo, W. S.; Wu, T.; Chen, H. Y. Hotspot-Induced Transformation of Surface-Enhanced Raman Scattering Fingerprints. *ACS Nano* **2010**, *4*, 3087–3094.
38. Tan, L. H.; Xing, S. X.; Chen, T.; Chen, G.; Huang, X.; Zhang, H.; Chen, H. Y. Fabrication of Polymer Nanocavities with Tailored Openings. *ACS Nano* **2009**, *3*, 3469–3474.
39. Lin, S.; Li, M.; Dujardin, E.; Girard, C.; Mann, S. One-Dimensional Plasmon Coupling by Facile Self-Assembly of Gold Nanoparticles into Branched Chain Networks. *Adv. Mater.* **2005**, *17*, 2553–2559.
40. Wang, X. J.; Li, G. P.; Chen, T.; Yang, M. X.; Zhang, Z.; Wu, T.; Chen, H. Y. Polymer-Encapsulated Gold-Nanoparticle Dimers: Facile Preparation and Catalytical Application in Guided Growth of Dimeric ZnO-Nanowires. *Nano Lett.* **2008**, *8*, 2643–2647.
41. Nye, J. F. Thermal-Behavior of Glacier and Laboratory Ice. *J. Glaciol.* **1991**, *37*, 401–413.
42. Mader, H. M. Observations of the Water-Vein System in Polycrystalline Ice. *J. Glaciol.* **1992**, *38*, 333–347.
43. Mader, H. M. The Thermal-Behavior of the Water-Vein System in Polycrystalline Ice. *J. Glaciol.* **1992**, *38*, 359–374.
44. Frens, G. Controlled Nucleation for Regulation of Particle-Size in Monodisperse Gold Suspensions. *Nat. Phys. Sci.* **1973**, *241*, 20–22.
45. Chen, T.; Chen, G.; Xing, S. X.; Wu, T.; Chen, H. Y. Scalable Routes to Janus Au-SiO(2) and Ternary Ag-Au-SiO(2) Nanoparticles. *Chem. Mater.* **2010**, *22*, 3826–3828.
46. See Supporting Information for details.
47. Xing, S. X.; Tan, L. H.; Yang, M. X.; Pan, M.; Lv, Y. B.; Tang, Q. H.; Yang, Y. H.; Chen, H. Y. Highly Controlled Core/Shell Structures: Tunable Conductive Polymer Shells on Gold Nanoparticles and Nanochains. *J. Mater. Chem.* **2009**, *19*, 3286–3291.
48. Gole, A.; Murphy, C. J. Azide-Derivatized Gold Nanorods: Functional Materials for "Click" Chemistry. *Langmuir* **2008**, *24*, 266–272.
49. Jain, P. K.; Eustis, S.; El-Sayed, M. A. Plasmon Coupling in Nanorod Assemblies: Optical Absorption, Discrete Dipole Approximation Simulation, and Exciton-Coupling Model. *J. Phys. Chem. B* **2006**, *110*, 18243–18253.
50. Chen, H. Y.; Abraham, S.; Mendenhall, J.; Delamarre, S. C.; Smith, K.; Kim, I.; Batt, C. A. Encapsulation of Single Small Gold Nanoparticles by Diblock Copolymers. *ChemPhysChem* **2008**, *9*, 388–392.
51. Chen, G.; Wang, Y.; Tan, L. H.; Yang, M. X.; Tan, L. S.; Chen, Y.; Chen, H. Y. High-Purity Separation of Gold Nanoparticle Dimers and Trimers. *J. Am. Chem. Soc.* **2009**, *131*, 4218–4219.
52. Kim, B. S.; Qiu, J. M.; Wang, J. P.; Taton, T. A. Magnetomicelles: Composite Nanostructures from Magnetic Nanoparticles and Cross-Linked Amphiphilic Block Copolymers. *Nano Lett.* **2005**, *5*, 1987–1991.
53. Yang, M. X.; Chen, T.; Lau, W. S.; Wang, Y.; Tang, Q. H.; Yang, Y. H.; Chen, H. Y. Development of Polymer-Encapsulated Metal Nanopartictes as Surface-Enhanced Raman Scattering Probes. *Small* **2009**, *5*, 198–202.
54. Xu, J.; Wang, H.; Liu, C. C.; Yang, Y. M.; Chen, T.; Wang, Y. W.; Wang, F.; Liu, X. G.; Xing, B. G.; Chen, H. Y. Mechanical Nanosprings: Induced Coiling and Uncoiling of Ultrathin Au Nanowires. *J. Am. Chem. Soc.* **2010**, *132*, 11920–11922.
55. Drenckhan, W.; Langevin, D. Monodisperse Foams in One to Three Dimensions. *Curr. Opin. Colloid Interface Sci.* **2010**, *15*, 341–358.
56. Nye, J. F.; Frank, F. C. Hydrology of the Intergranular Veins in a Temperate Glacier. *International Assoc. of Sci. Hydrology Pub. 95 (Symposium at Cambridge 1969-Hydrology of Glaciers)* **1973**, 157–161.
57. Deville, S.; Saiz, E.; Nalla, R. K.; Tomsia, A. P. Freezing as a Path to Build Complex Composites. *Science* **2006**, *311*, 515–518.
58. Zhang, H. F.; Hussain, I.; Brust, M.; Butler, M. F.; Rannard, S. P.; Cooper, A. I. Aligned Two- and Three-Dimensional Structures by Directional Freezing of Polymers and Nanoparticles. *Nat. Mater.* **2005**, *4*, 787–793.
59. Estevez, L.; Kelarakis, A.; Gong, Q. M.; Da'as, E. H.; Giannelis, E. P. Multifunctional Graphene/Platinum/Nafion Hybrids *via* Ice Templating. *J. Am. Chem. Soc.* **2011**, *133*, 6122–6125.
60. Zhang, H.; Lee, J. Y.; Ahmed, A.; Hussain, I.; Cooper, A. I. Freeze-Align and Heat-Fuse: Microwires and Networks from Nanoparticle Suspensions. *Angew. Chem., Int. Ed.* **2008**, *47*, 4573–4576.